Journal of Hazardous Materials 187 (2011) 509–516

Contents lists available at ScienceDirect

Journal of Hazardous Materials

journal homepage: www.elsevier.com/locate/jhazmat

# Enhanced visible light photocatalytic activity of novel Pt/C-doped $TiO_2$/$PtCl_4$ three-component nanojunction system for degradation of toluene in air

Fan Dong[a,b,c], Haiqiang Wang[a,c], Guo Sen[a,c], Zhongbiao Wu[a,c,*], S.C. Lee[d]

[a] Department of Environmental Engineering, Zhejiang University, Hangzhou 310027, PR China
[b] College of Environmental and Biological Engineering, Chongqing Technology and Business University, Chongqing, 400067, PR China
[c] Zhejiang Provincial Engineering Research Center of Industrial Boiler & Furnace Flue Gas Pollution Control, Hangzhou, 311202, PR China
[d] Department of Civil and Structural Engineering, Research Center for Environmental Technology and Management, The Hong Kong Polytechnic University, Hong Kong, China

ARTICLE INFO

*Article history:*
Received 1 December 2010
Received in revised form 12 January 2011
Accepted 13 January 2011
Available online 19 January 2011

*Keywords:*
C-doped $TiO_2$
Visible light
Photocatalytic activity
Nanojunction
Platinum
Toluene

ABSTRACT

C-doped $TiO_2$ nanoparticles prepared by partial oxidation of TiC were modified with Pt species by impregnation–calcination method in order to enhance the visible light photocatalytic activity. The physicochemical properties of as-prepared samples were characterized by various techniques in detail. The results indicated that a novel Pt/C-doped $TiO_2$/$PtCl_4$ three-component nanojunction system was formed, where C-doped $TiO_2$ and $PtCl_4$ behaved as two visible light responsive components, and Pt metal as electron-transfer system. The three-component nanojunctioned photocatalyst system exhibited six times higher visible light activity than that of the pristine C-doped $TiO_2$ in degradation of toluene in air. The dramatically enhanced activity can be attributed to the increased utilization of visible light, the enhanced charge carrier separation and transfer process. Further more, the band structure and photocatalysis mechanism over the three-component nanojunction system was proposed and discussed. This work may provide new insights into the design of novel multi-component photocatalyst system with efficient visible light activity.



## 1. Introduction

Visible light induced photocatalysis has attracted intensive interest due to its potential applications in environmental pollutants purification and solar energy conversion by utilizing visible light in solar or indoor light [1–6]. The leading candidate photocatalyst, $TiO_2$, however, requires ultraviolet light (about 5% of natural solar light) for electron–hole separation due to its relatively wide band gap (ca. 3.2 eV for anatase $TiO_2$). Nonmetal doping, such as C and N doping, has displayed promising results in extending the light absorption of $TiO_2$ into visible light (about 43% of the natural solar light) region [7–25]. Numerous contributions have been devoted recently to developing effective nonmetal-doped $TiO_2$ based single-component photocatalysts with visible light response [7–25].

However, nonmetal doping intrinsically leads to the serious problem of massive charge carrier recombination of $TiO_2$, which largely limits the visible light photocatalysis efficiency of nonmetal-doped $TiO_2$ [26,27]. From the viewpoint of energetic or environmental applications, higher reaction efficiency is required because the photocatalytic efficiency of current nonmetal-doped $TiO_2$ under visible light irradiation is still low [28–30].

Recently, $TiO_2$-based three-component systems have been constructed to greatly improve the visible light photocatalytic performance, where every component plays a separate role in the photocatalytic process [31–33]. The pioneering work is reported by Tada et al. [31], who has revealed that CdS–Au–$TiO_2$ three-component nanojunction system exhibits a high photocatalytic activity, as a result of vectorial electron transfer driven by the two-step excitation of $TiO_2$ and CdS. Choi and co-workers [32] organized ternary CdS/$TiO_2$/Pt hybrid photocatalysts for visible light-induced hydrogen production, where CdS functions as visible light responsive component and Pt metal are beneficial for efficient interfacial charge transfer and separation. This three-component nanojunction system has the vectorial electron transfer process of CdS → $TiO_2$ → Pt. Hu et al. [33] also constructed ternary AgBr–Ag–$TiO_2$ system as visible light photocatalyst for the destruction of the organic pollutant and bacteria, where AgBr is the visible light responsive component and the metal Ag species on the surface contributed to the enhanced the electron–hole separation and interfacial charge transfer. These studies provide novel route to enhance the visible light photocatalytic activity of pure $TiO_2$, demonstrating that the development of better visible light photocatalysts depends on a wide range of visible light response and effective interfacial charge transfer and separation [34]. Thus, it is

* Corresponding author at: Department of Environmental Engineering, Zhejiang University, Hangzhou 310027, PR China. Tel.: +86 571 87952459; fax: +86 571 87953088.
*E-mail address:* zbwu@zju.edu.cn (Z. Wu).

0304-3894/$ – see front matter © 2011 Elsevier B.V. All rights reserved.
doi:10.1016/j.jhazmat.2011.01.062

still desirable to design novel visible light $TiO_2$-based photocatalytic system with broadened visible light response and improved charge carrier separation. However, there are few reports on nanojunctioned multi-component photocatalyst system based on nonmetal doped $TiO_2$ with visible light activity. It is highly possible to construct such photocatalyst system with efficient visible light activity based on nonmetal doped $TiO_2$.It is known that, photosensitizing with noble metal complex (e.g., $PtCl_4$ and $H_2PtCl_6$) is an effective method for enhancing the visible light response $TiO_2$-based photocatalyst [35–37]. Moreover, the deposition of a noble metal (Pt or Au), on the surface of $TiO_2$ at nanoscale highly improved its photocatalytic efficiency through the Schottky barrier by conduction band electron trapping, which increases the charge carrier separation rate [38–40].

Inspired by the above interesting work, we constructed Pt/C-doped $TiO_2$/$PtCl_4$ three-component nanojunction system by a facile impregnation–calcination method based on single-component C-doped $TiO_2$ with visible light response, where $PtCl_4$ enhances the visible absorbance and Pt metal behaves as the electron transfer system in order to broaden the range of visible light response and improve the separation of charge carrier simultaneously. Different from previous research, both C-doped $TiO_2$ and $PtCl_4$ are photochemical systems that can be excited by visible light. The novel Pt/C-doped $TiO_2$/$PtCl_4$ three-component nanojunction system exhibits enhanced visible light photocatalytic activity in degradation of toluene in gas phase.

## 2. Experimental

### 2.1. Preparation of photocatalysts

C-doped $TiO_2$ nanocrystals (C-$TiO_2$) were prepared by partial oxidation of TiC [27]. In a typical process, 3.0 g TiC powder was loaded in a ceramic crucible, and then placed in the middle of muffle furnace which was open to the atmosphere. The temperature was slowly ramped up to 400 °C at a rate of 2 °C/min and kept for 2 h to obtain C-doped $TiO_2$. Pt loading was performed by incipient impregnation of C-doped $TiO_2$ with aqueous solutions of $H_2PtCl_6$ at room temperature, followed by stirring for 1 h and heating at 150 °C for water evaporation. Finally, the sample was treated at 300 °C for 1 h. The amount of loaded platinum was controlled at 0, 0.01, 0.05, 0.2, 0.5 and 1.0 wt%. The as-prepared samples were labeled as Pt/C-$TiO_2$/$PtCl_4$-*x*, where *x* represented the content of Pt.

### 2.2. Characterization

The crystal phase of the samples was analyzed by X-ray diffraction with Cu Kα radiation (XRD: model D/max RA, Rigaku Co., Japan). Raman spectra were recorded at room temperature using a micro-Raman spectrometer (Raman: RAMANLOG 6, USA) with a 514.5 nm $Ar^+$ laser as the excitation source in a backscattering geometry. X-ray photoelectron spectroscopy with Al Kα X-rays ($h\nu$ = 1486.6 eV) radiation (XPS: Thermo ESCALAB 250, USA) was used to investigate the surface properties of the samples. The shift of the binding energy was corrected using the C1s level at 284.8 eV as an internal standard. The morphology, structure and crystal size of the samples were examined by transmission electron microscopy (TEM: JEM-2010, Japan). The UV–vis diffuse reflection spectra were obtained for the dry-pressed disk samples using a Scan UV–vis spectrophotometer (UV–vis DRS: TU-1901, China) equipped with an integrating sphere assembly, using $BaSO_4$ as reflectance sample. The photoluminescence spectra were measured with a fluorospectrophotometer (PL: Fluorolog-3-Tau, France) using a Xe lamp as excitation source with optical filter.

### 2.3. Tests of photocatalytic activities

Photocaytalytic degradation of toluene in air is chosen as the probe reaction to test the activities of the as-prepared samples, as toluene is considered as a typical indoor pollutant [41,42]. The photocatalytic activity tests were performed at room temperature using a 1.8 L photo-reactor. The catalyst was prepared by coating an ethanol suspension of the catalyst onto a dish with a diameter of 12.5 cm. The weight of catalyst used for each test was kept at 0.20 g. The dish containing catalyst was dried at 60 °C for 1 h to evaporate the ethanol and then cooled to room temperature before being used. After the catalyst-coated dish was placed in the reactor, a small amount of toluene was injected into the reactor with a micro-syringe. The analysis of toluene concentration in the reactor was conducted with a GC-FID (FULI 9790, China). The toluene vapor was allowed to reach adsorption equilibrium in the reactor prior to irradiation. The initial concentration of toluene after adsorption equilibrium was controlled at 150 mg/$m^3$, respectively. A 150 W Xe lamp with an IR cutoff and a UV-cutoff optical filter ($\lambda$ < 425 nm) was placed above the reactor as the light source. The temperature of the reactor was controlled at 25 ± 1 °C by continuous cooling air. The RH was controlled at 60%.

The photocatalytic activity of the catalyst samples can be quantitatively evaluated by comparing the apparent reaction rate constants (*k*). The photocatalytic oxidation of toluene in gas phase is a pseudo-first-order reaction and its kinetics can be expressed as follows: $\ln(C_0/C) = kt$, $C_0$ and $C$ are the initial concentration and the reaction concentration of toluene, respectively [43,44].

## 3. Results and discussion

### 3.1. Visible light photocatalyic activities

Fig. 1a shows the photocatalytic activities of C-$TiO_2$ and Pt/C-$TiO_2$/$PtCl_4$ samples under visible light irradiation in degradation of gaseous toluene by plotting of $\ln(C_0/C)$ versus *t*. It can be seen that the assumption of pseudo-first order reaction is valid. C-$TiO_2$ sample exhibits decent visible light activity due to carbon doping (*k*, 0.0025 $min^{-1}$). The toluene degradation percentage in 120 min is 27.5%. With the different content of Pt species in rang of 0.01–1.0%, all Pt/C-$TiO_2$/$PtCl_4$ samples exhibit more efficient visible light activity than that of unmodified C-$TiO_2$. Under optimized condition, the toluene degradation percentage in 120 min reaches 87.4%, indicating the great enhancement of activity by Pt surface modification (*k*, 0.0171 $min^{-1}$). Fig. 1b shows the relationship between apparent rate constant (*k*) and the weight ratio of Pt. From the result, it is observed that the photocatalytic efficiency (*k* value) increases with increase in the Pt loading upon certain level (optimal Pt loading content) and then decreases. The optimized loading content of Pt species is found to be 0.5 wt%. The visible light activity of the optimal catalyst is about six times higher than that of C-$TiO_2$. The excess loading of Pt species may cover the active sites on C-$TiO_2$ surface thereby reducing the photocatalytic efficiency. These results suggest that loading Pt species on the surface of C-doped $TiO_2$ could promote the visible light photocatalytic activity significantly. To the best of our knowledge, there is no report on the promotive effect of Pt species on C-doped $TiO_2$.

### 3.2. XPS analysis

In order to determine the chemical state of the elements and total density of states (DOS) of the valence band (VB), XPS measurement is carried out in pristine C-$TiO_2$ and Pt/C-$TiO_2$/$PtCl_4$-1.0% samples. Fig. 2a shows the binding energy for Pt4f spectrum of Pt/C-$TiO_2$/$PtCl_4$-1.0% sample, which exhibits three different types

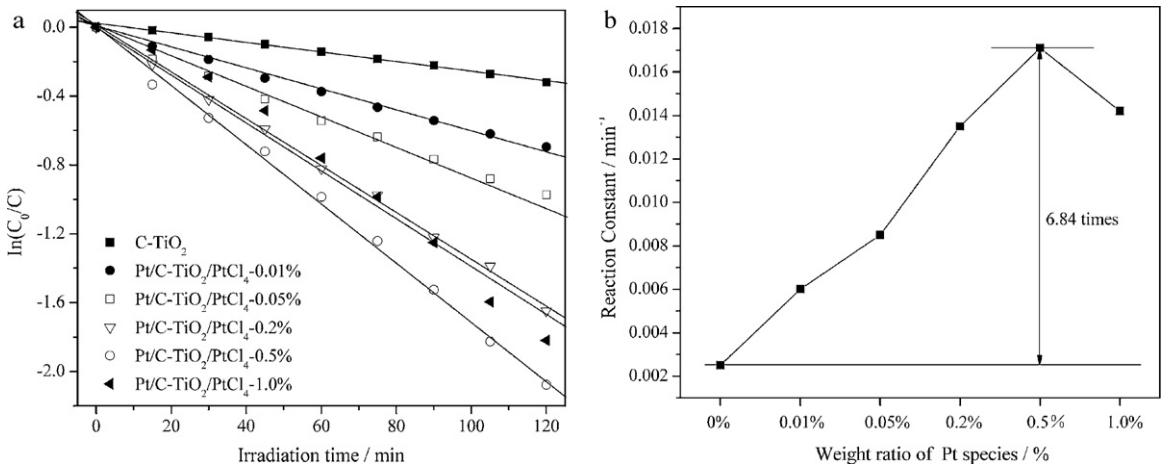


**Fig. 1.** (a) Photocatalytic activities of C-$TiO_2$ and Pt/C-$TiO_2$/$PtCl_4$ samples under visible light irradiation, (b) the relationship between apparent rate constant ($k$) and the weight ratio of Pt.

of doublet peaks ($4f_{5/2}$ and $4f_{7/2}$) at 78.2 and 74.9 eV for Pt(IV), at 76.2 and 72.9 eV for Pt(II), at 74.3 and 70.0 eV for Pt(0) [45,46]. The surface content of Pt(IV), Pt(II) and Pt(0) is 0.07, 0.23 and 0.07 atm.% respectively. It was reported that calcination of Pt chloride precursor at a higher temperature produces metal Pt particles on the oxide surface [47]. Therefore, a certain amount of Pt(0) is generated on the our sample. The generation of Pt(II) seems to be unusual. However, Li et al. and Zhao et al. also observed Pt(II) in their impregnated prepared Pt(IV)/$TiO_2$ samples [36,48]. Accordingly, It is very likely that the Pt(II) species is produced from Pt(IV) during the work-up of the XPS sample [48,49]. Therefore, the chemical state of Pt species existed on the surface of C-$TiO_2$ are actually Pt(IV) and Pt(0). The Cl2p peak at 198–202 eV is observed on Pt/C-$TiO_2$/$PtCl_4$-1.0% sample (Fig. 2b). The ratio of [Pt(IV) + Pt(II)]/$Cl^-$ is 4.1, indicating that Pt(IV) existed as $PtCl_4$.

The DOS of VB in C-$TiO_2$ and Pt/C-$TiO_2$/$PtCl_4$-1.0% samples from VB XPS is shown in Fig. 2c. The dispersed electronic states below 3.0 eV are observed above the valence band edge for both samples.

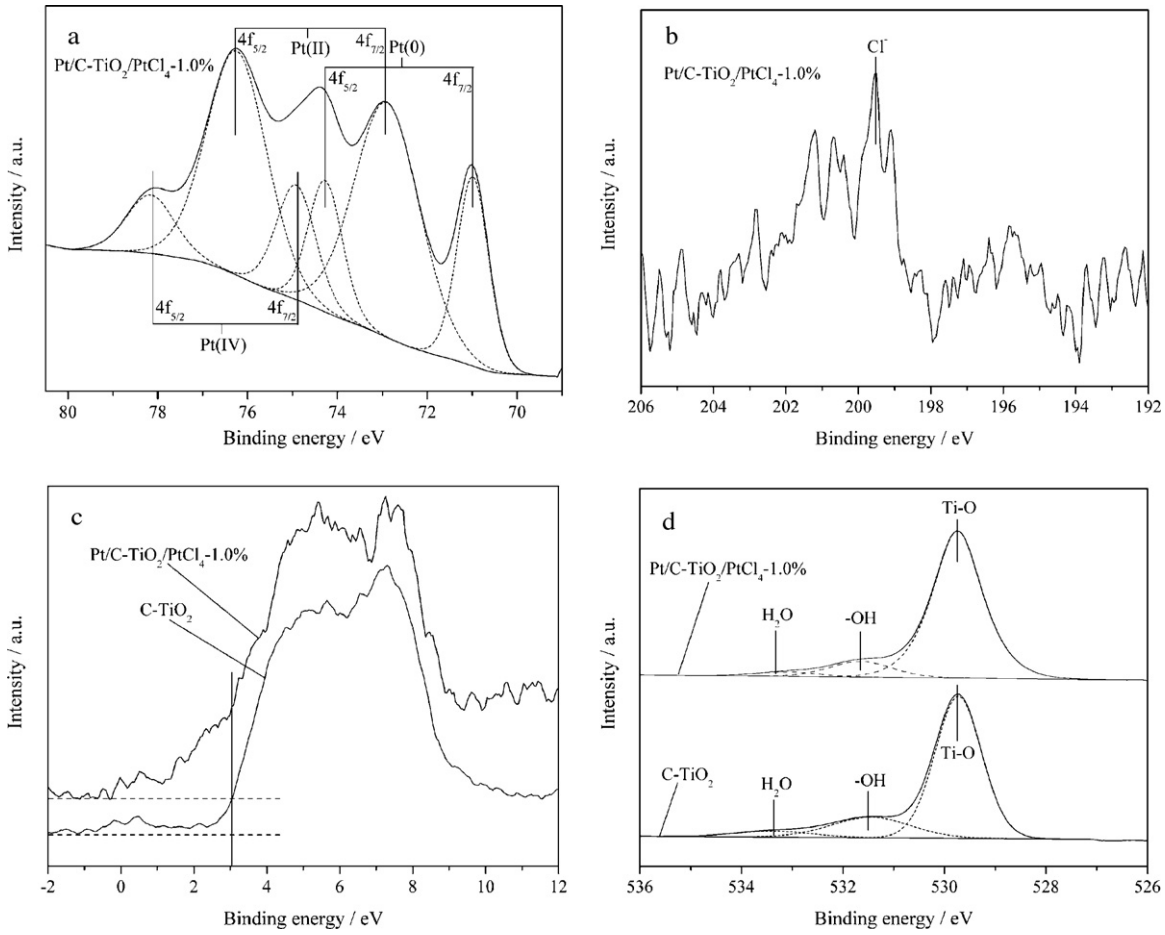


**Fig. 2.** XPS spectra for (a) Pt4f, (b) Cl2p, (c) VB and (d) O1s region of C-$TiO_2$ and Pt/C-$TiO_2$/$PtCl_4$-1.0% samples.

**Table 1**
Curve-fitting result of high-resolution XPS spectra for O1s.

| Sample | O1s (Ti–O) | O1s (–OH) | O1s ($H_2O$) |
|---|---|---|---|
| C-$TiO_2$ | | | |
| $E_b$ (eV) | 529.7 | 531.5 | 533.4 |
| $r_i$ (%) | 76.0 | 18.7 | 5.3 |
| Pt/C-$TiO_2$/$PtCl_4$-1.0% | | | |
| $E_b$ (eV) | 529.7 | 531.6 | 533.1 |
| $r_i$ (%) | 86.2 | 10.8 | 3.0 |

For C-$TiO_2$ sample, these states can be attributed to the contribution of C2p orbitals, which are directly responsible for the electronic origin of band gap narrowing and visible light photoactivity of the C-doped $TiO_2$ [50,51]. The electronic states of Pt/C-$TiO_2$/$PtCl_4$-1.0% sample are more widely dispersed above 1.5 eV, which can be ascribed to superimposing of the VB DOS of $PtCl_4$ and C-$TiO_2$ [46].

The XPS spectra of O1s region for C-$TiO_2$ and Pt/C-$TiO_2$/$PtCl_4$-1.0% samples are shown in Fig. 2d. Fig. 2d and Table 1 indicate that the O1s region of for both samples can be fitted into three peaks, which can be attributed to Ti–O, –OH hydroxyl groups and chemisorbed $H_2O$, respectively [52]. The $r_i$ (%) in Table 1 indicates the atomic ratio of each contribution to all kinds oxygen contributions. It can be seen that the $r_{-OH}$ (%) of Pt modified sample is lower that of pristine C-$TiO_2$. This can be explained by the fact that platinum chloride strongly interacts with Ti–OH to form Ti–O–$PtCl_4$, which consumes some –OH on the catalyst surface [53].

### 3.3. Phase structure

The XRD patterns of as-prepared samples are shown in Fig. 3a. The phase structure in C-$TiO_2$ and Pt/C-$TiO_2$/$PtCl_4$ samples consists of anatase (JCPDS file No. 21-1272) and rutile phase (JCPDS, file No. 77-442). No Pt or $PtCl_4$ related diffraction peaks could be observed in Pt/C-$TiO_2$/$PtCl_4$ samples, which can be ascribed to the few Pt amounts and that the Pt species are uniformly dispersed on the surface of C-$TiO_2$. Fig. 3a also indicates that Pt modification has almost no influence on the phase structure of C-$TiO_2$ with 70% rutile and 30% anatase. By using the Debye-Scherrer equation, the crystallite sizes of anatase and rutile phase are calculated to be 20.1 and 30.5 nm, respectively.

Raman spectra of C-$TiO_2$, selected Pt/C-$TiO_2$/$PtCl_4$ samples are shown Fig. 3b. The observed characteristic Raman bands at 144, 196, 395, 515, and 638 $cm^{-1}$, assigned to the $E_g$, $B_{1g}$, $A_{1g}$, $B_{2g}$, and $E_g$ vibrational modes of $TiO_2$, indicates the presence of the anatase phase in all these samples [54]. The typical Raman bands due to rutile phase appear at 143 (superimposed with the 144 $cm^{-1}$ band of anatase phase), 235, 447, and 612 $cm^{-1}$, which can be ascribed to the $B_{1g}$, two-phonon scattering, $E_g$, and $A_{1g}$ modes of rutile phase, respectively [55]. The band at 144 $cm^{-1}$ is the strongest one for the anatase phase and the band at 143 $cm^{-1}$ is the weakest one for the rutile phase. No Raman bands relevant to Pt or $PtCl_4$ are observed, which further confirm the XRD result.

### 3.4. Microstructure and morphology

To obtain information about the structure of the samples, TEM observation of C-$TiO_2$ and Pt/C-$TiO_2$/$PtCl_4$-1.0% was carried out. From the TEM image (Fig. 4a), C-$TiO_2$ sample consists of agglomerates of primary particles of 20–30 nm in diameter. The uniform lattice fringes can be observed over an entire primary particle (Fig. 4b), indicating the good crystallization. Different from C-$TiO_2$ sample, some Pt nanoparticles (about 5 nm) are found dispersed on the surface of Pt/C-$TiO_2$/$PtCl_4$-1.0% sample (Fig. 4c). The HRTEM images show the lattice fringes of $d$ = 0.322 and 0.224 nm in Fig. 4d well matched with the crystallographic planes of rutile $TiO_2$ (1 1 0) and face-centered cubic (fcc) Pt (1 1 1), respectively [17,56,57]. The insets in Fig. 4d show the corresponding fast Fourier transform (FFT) patterns of metal Pt and C-$TiO_2$ with crystal growth orientation.

According to the XPS result, the Pt nanoparticles come from the decomposition of platinum chloride precursor at a higher temperature. The intimate contact between Pt nanoparticle and C-$TiO_2$ favors the formation of nanodimensional junction between the two components. $PtCl_4$ can not be observed by TEM, because $PtCl_4$ exists as $Pt^{4+}$ and $Cl^-$ ions. The existence of $PtCl_4$ on catalyst surface, however, is confirmed by XPS. Thus, the as-prepared Pt-modified sample actually consists of three components, forming novel Pt/C-$TiO_2$/$PtCl_4$ nanojunction system.

### 3.5. UV–vis DRS and PL

Fig. 5a shows UV–vis DRS of C-$TiO_2$, Pt/C-$TiO_2$/$PtCl_4$ samples and P25. Compared to P25, C-$TiO_2$ exhibits strong visible light absorption. The absorption of visible light region in the spectrum of C-$TiO_2$ is caused by the excitation of electrons from modified valence band in the band gap due to carbon doping. When the amount of Pt species was less than 0.20 wt.%, no obvious change in visible light absorption was observed compared with C-$TiO_2$. Significant increase in absorbance of visible light can be observed when the content of Pt species is greater than 0.50 wt.%. It was reported that modification of $TiO_2$ by $PtCl_4$ could make it absorb visible light [58,59]. The increase in visible light absorption is assignable to the charge transfer from the ligand ($Cl^-$) to Pt(IV) ions [58,59]. These results indicate that $PtCl_4$ behaves as a photosensitizer to make C-$TiO_2$ absorb more visible light through the surface modification. The

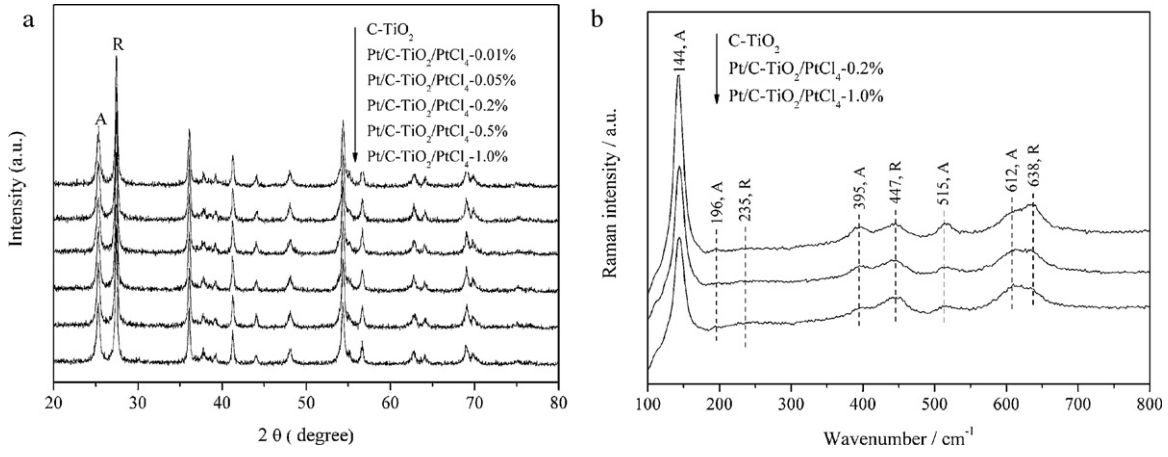


**Fig. 3.** XRD patterns (a) of C-$TiO_2$ and Pt/C-$TiO_2$/$PtCl_4$ samples, and Raman spectra (b) of C-$TiO_2$ and selected Pt/C-$TiO_2$/$PtCl_4$ samples (A: anatase, R: rutile).

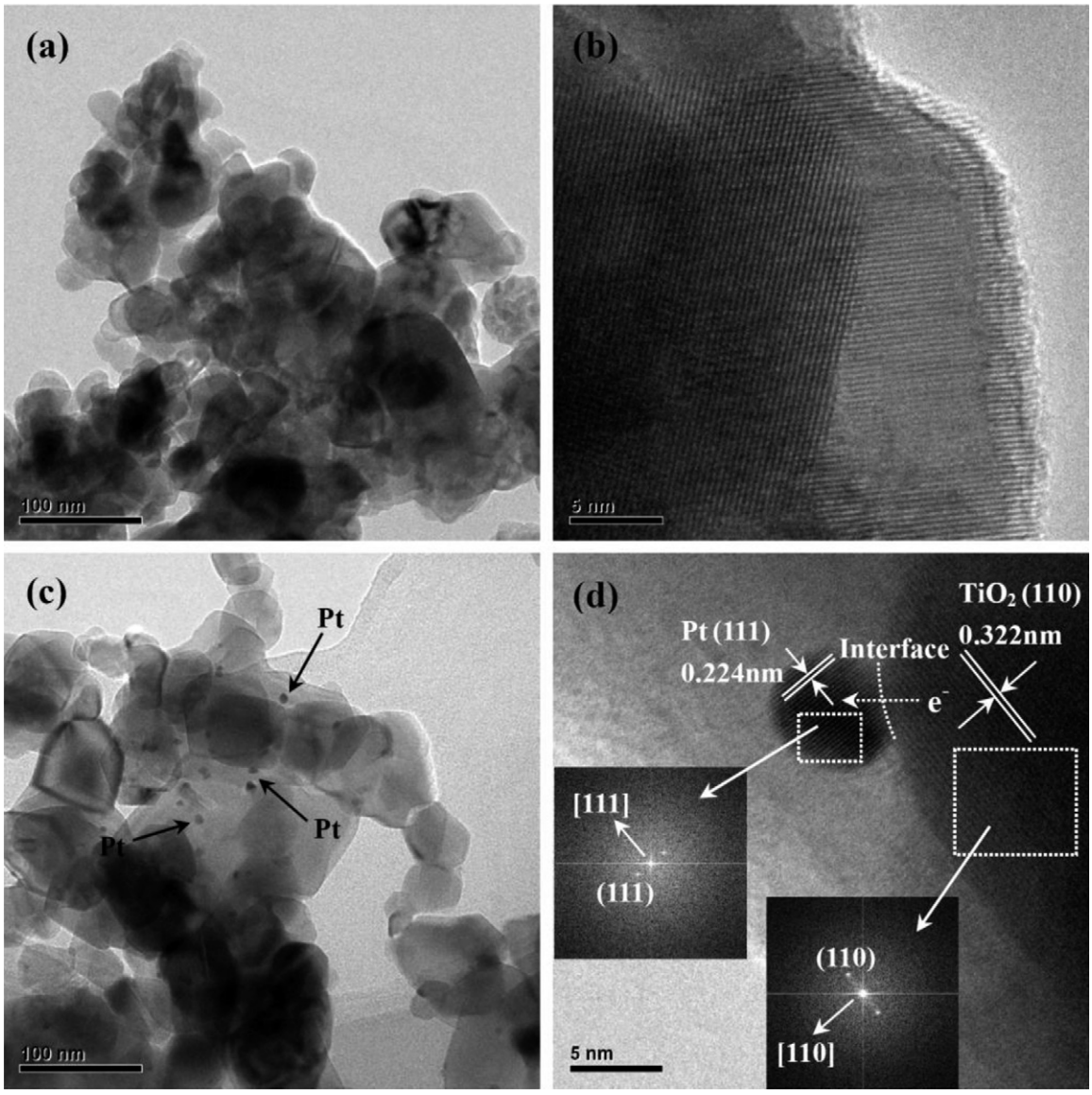


**Fig. 4.** TEM and HRTEM images of (a and b) C-$TiO_2$ and (c and d) Pt/C-$TiO_2$/$PtCl_4$-1.0% sample. Inset in (d) shows the FFT patterns of metal Pt and C-$TiO_2$.

absorption band of $PtCl_4$ superimposed with that of C-$TiO_2$. Generally, the photocatalytic activity is proportional to $(I_\alpha \Phi)^n$ ($n = 1$ for low light intensity and $n = 1/2$ for high light intensity), where $I_\alpha$ is the photo numbers absorbed by photocatalyst per second and $\Phi$ is the efficiency of the band gap transition [60]. The enhanced visible light photocatalytic activity of Pt/C-$TiO_2$/$PtCl_4$ system can be partly explained in terms of an increase in $I_\alpha \Phi$ resulting from the broadened absorption in the visible light region.

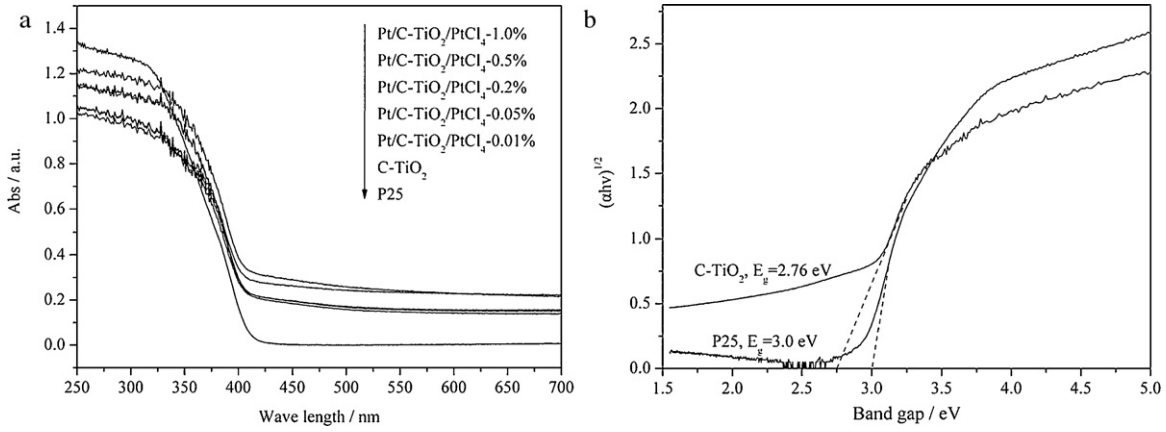


**Fig. 5.** (a) UV–vis DRS of C-$TiO_2$, Pt/C-$TiO_2$/$PtCl_4$ samples and P25, (b) Plot of $(\alpha h\nu)^{1/2}$ vs. photon energy of P25 and C-$TiO_2$.

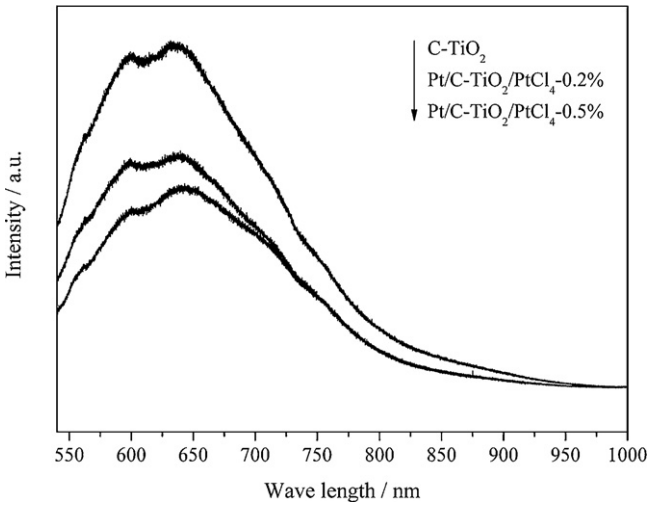


**Fig. 6.** PL spectra of C-$TiO_2$ and selected Pt/C-$TiO_2$/$PtCl_4$ samples (Excitation light: 514.5 nm).

The band gap ($E_g$) energies can be estimated from UV–vis DRS spectra. The relation between absorption coefficient ($\alpha$) and incident photon energy ($h\nu$) can be written as $\alpha h\nu = B_d(h\nu - E_g)^{1/2}$ for allowed indirect transition, where $B_d$ is the absorption constants [15]. Plot of $(\alpha h\nu)^{1/2}$ versus $h\nu$ from the spectra data of C-$TiO_2$ and P25 in Fig. 5a are presented in Fig. 5b. The $E_g$ estimated from the intercept of the tangents to the plots is 2.76 and 3.0 eV for C-$TiO_2$ and P25, respectively. Carbon doping reduces the band gap of $TiO_2$ by lifting the position of valence band, as evidenced by VB XPS [11,15].

Photoluminescence (PL) emission spectra have been widely used to investigate the efficiency of charge carrier trapping, migration, and transfer in order to understand the fate of electron–hole pairs in semiconductor particles since PL emission results from the recombination of free carriers [15,28]. Fig. 6 shows the room-temperature PL spectra of C-$TiO_2$ and selected Pt/C-$TiO_2$/$PtCl_4$ samples under visible light (514.5 nm) irradiation. As the PL emission is the result of the recombination of excited electrons and holes, the lower PL intensity indicates the increased in charge separation rate, thus higher photocatalytic activity [28]. It can be seen from Fig. 6 that the PL intensity of Pt/C-$TiO_2$/$PtCl_4$ samples is lower than that of C-$TiO_2$, although the visible light absorption of the former is stronger than that of the latter (Fig. 5a). It is well known that the Pt particle deposited on the $TiO_2$ at nanoscale surface produced the Schottky barrier that facilitated the electron capture [38–40]. Under visible light irradiation, the photo-generated electrons from C-$TiO_2$ and $PtCl_4$ can be trapped by metal Pt on the surface through the schottky barrier effect, which could enhance the charge carrier separation. The electrons then migrated to $O_2$ molecules adsorbed on the surface of the Pt particle, generating $O_2^{\bullet-}$ species. Thus, the enhanced charge separation in Pt/C-$TiO_2$/$PtCl_4$ samples can be ascribed to the promotion effect of Pt particle on catalyst surface, forming nanojunction system (Fig. 4d), which is another reason for the enhanced visible light photocatalytic activity of Pt/C-$TiO_2$/$PtCl_4$ samples.

**Table 2**
The calculated conduction band (CB) edge, valence band (VB) position and band gap energy for P25 and C-doped $TiO_2$ at the point of zero charge.

| Semiconductors | Absolute electronegativity ($X$) (/eV) | Calculated CB position (/eV) | Calculated VB position (/eV) | Band gap energy $E_g$ (/eV) |
|---|---|---|---|---|
| P25 | 5.81 | −0.19 | 2.81 | 3.0 |
| C-doped $TiO_2$ | – | −0.19 | 2.57 | 2.76 |

### 3.6. Band structure and photocatalysis mechanism of Pt/C-$TiO_2$/$PtCl_4$ nanojunction system

The band edge positions of conduction band (CB) and valence band (VB) of semiconductor can be determined with the following approach. The conduction band edge ($E^0_{CB}$) of a semiconductor at the point of zero charge ($pH_{ZPC}$) can be predicted by the equation $(E^0_{CB}) = X - E^C - 1/2E_g$ where $X$ is the absolute electronegativity of the semiconductor ($X$ is 5.81 eV for P25 $TiO_2$; $X$ is unknown for C-doped $TiO_2$) [61–63]. $E_C$ is the energy of free electrons on the hydrogen scale (~4.5 eV). $E_g$ is the band gap energy of the semiconductor. The calculated position of CB and VB of P25 are listed in Table 2. It is well known that nonmetal doping does not change the CB position of $TiO_2$. The VB position of C-doped $TiO_2$ can be calculated based on the caculated CB position of $TiO_2$ and $E_g$ of C-doped $TiO_2$, as also shown in Table 2. According to the photoelectrochemical study results of platinum (IV) chloride surface modified $TiO_2$ by Kisch and co-workers, the redox potentials of $Pt_{IV/III}$ couple and Pt-Cl/$Cl^-$ are estimated to be −0.4 eV and 1.6 V, respectively [64].

On the basis of their energy band diagram, the schematic electronic band structure and photocatalytic process of Pt/C-$TiO_2$/$PtCl_4$ nanojunction system can be proposed, as shown in Fig. 7. Two important redox potentials of $O_2/O_2^{\bullet-}$ and $OH^{\bullet}/-OH$ are also displayed on this illustration.

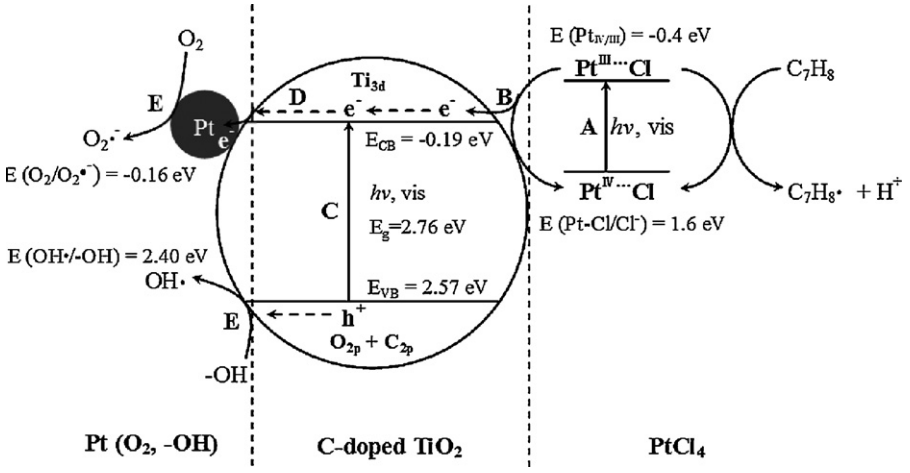


**Fig. 7.** Schematic illustration of the band structure and photocatalysis mechanism over Pt/C-$TiO_2$/$PtCl_4$ nanojunction system.

Since both C-doped $TiO_2$ and $PtCl_4$ can be excited by visible light and have different photoabsorption ranges, the conjunction of their photoabsorption can broaden the range of visible-light absorption (Fig. 5a). The photocatalytic reaction is initiated by the absorption of visible-light photons. Local excitation of the $PtCl_4$ by visible light affords charge transfer-ligand-to-metal, which both undergo homolytic Pt–Cl bond cleavage to yield Pt(III) and a chlorine atom (process A), as also observed by Kisch and co-workers [37]. The labile platinum(III) intermediate will rapidly transfer an electron to the CB of C-$TiO_2$ (process B), while the chlorine atom abstracts an electron from the oxygen lattice. At the same time, visible light irradiation of C-$TiO_2$ results in the creation of photogenerated holes in its VB and electrons in its CB (process C). CB-electrons from both C-$TiO_2$ and $PtCl_4$ can easily transfer to the metal Pt (see the interface in Fig. 4d) through the Schottky barrier (process D), which is consistent with the previous study on electron transfer from $TiO_2$ to metal Pt clusters [38–40]. In this way, the photogenerated electrons and holes are efficiently separated (Fig. 6). The VB-holes in C-$TiO_2$ and electrons trapped by metal Pt react with $OH^-$ and molecule $O_2$ on the catalyst surface to form $OH^\bullet$ radicals and $O_2^{\bullet-}$ superoxide anion radicals, respectively (process E and F). The photogenerated hole-based oxidation is thought to play an important role in photocatalytic reaction [36]. The $O_2^{\bullet-}$ radicals then interact with adsorbed $H_2O$ to produce more $OH^\bullet$ radicals, which are known to be the most oxidizing species [22]. These $OH^\bullet$ radicals then react with gaseous toluene to mineralize it [22].

On the basis of above results, we attributed the enhancement in the photocatalytic activity of Pt/C-$TiO_2$/$PtCl_4$ to the increased capabilities of visible-light absorption and enhanced charge separation and transfer process due to formation of three-component nanojunction system [34]. Thus, our result may provide new insights into the development of novel multi-component photocatalyst system with high visible light activity.

## 4. Conclusion

In summary, the visible light-driven C-doped $TiO_2$ prepared by partial oxidation of TiC was further modified with Pt species by a facile impregnation–calcination method in order to enhance the visible light activity. Various characterization tools confirmed the formation of novel three-component Pt/C-doped $TiO_2$/$PtCl_4$ nanojunction system, where C-doped $TiO_2$ and $PtCl_4$ functioned as two visible light responsive components, and Pt metal as electron transfer and separation system. The range of visible light response of the three-component nanojunction system is broadened and the charge carrier separation is enhanced simultaneously. This photocatalyst system exhibited six times higher activity than that of pristine C-doped $TiO_2$ under visible light irradiation for degradation of toluene in air. The proposed band structure and photocatalysis mechanism suggested that the increased utilization of visible light, the enhanced charge carrier separation and transfer process were mainly responsible for the enhanced visible light photocatalytic activity of the novel three-component nanojunction system. Therefore, our research result could provide new perspective on designing high-performance visible light photocatalyst system with multi-components for environmental pollution control.

## Acknowledgements

This research is funded by National High Technology Research and Development Program ('863'Program) of China (J20100308), Zhejiang Provincial Engineering Research Center of Industrial Boiler & Furnace Flue Gas Pollution Control (No. 2010B01), Changjiang Scholar Incentive Program (Ministry of Education, China, 2009) and National Natural Science Foundation of China (NSFC-50808156). This work is also supported by The Program for Chongqing Innovative Research Team Development in University (KJTD201020) and The Chongqing Key Natural Science Foundation (CSTC, 2008BA4012). This work was also funded by the Research Grants Council of Hong Kong (PolyU 5204/07E and PolyU 5175/09E), and The Hong Kong Polytechnic University (GU712, GYX75 and GYX0L).

## References

[1] X.B. Chen, S.S. Mao, Titanium dioxide nanomaterials: synthesis, properties, modifications, and applications, Chem. Rev. 107 (2007) 2891–2959.
[2] A. Fujishima, X.T. Zhang, D.A. Tryk, $TiO_2$ photocatalysis and related surface phenomena, Surf. Sci. Rep. 63 (2008) 515–582.
[3] A. Kudo, Y. Miseki, Heterogeneous photocatalyst materials for water splitting, Chem. Soc. Rev. 38 (2009) 253–278.
[4] H.J. Zhang, G.H. Chen, D.W. Bahnemann, Photoelectrocatalytic materials for environmental applications, J. Mater. Chem. 19 (2009) 5089–5121.
[5] S. Rehman, R. Ullah, A.M. Butt, N.D. Gohar, Strategies of making $TiO_2$ and ZnO visible light active, J. Hazard. Mater. 170 (2009) 560–569.
[6] J.H. Mo, Y.P. Zhang, Q.J. Xu, J.J. Lamson, R.Y. Zhao, Photocatalytic purification of volatile organic compounds in indoor air: a literature review, Atmos. Environ. 43 (2009) 2229–2246.
[7] S.U.M. Khan, M. Al-Shahry, W.B. Ingler Jr., Efficient photochemical water splitting by a chemically modified n-$TiO_2$, Science 297 (2002) 2243–2245.
[8] S. Sakthivel, H. Kisch, Daylight photocatalysis by carbon-modified titanium dioxide, Angew. Chem., Int. Ed. 42 (2003) 4908–4911.
[9] S. Bangkedphol, H.E. Keenan, C.M. Davidson, A. Sakultantimetha, W. Sirisaksoontornc, A. Songsasen, Enhancement of tributyltin degradation under natural light by N-doped $TiO_2$ photocatalyst, J. Hazard. Mater. 184 (2010) 533–537.
[10] H. Liu, A. Imanishi, Y. Nakato, Mechanisms for photooxidation reactions of water and organic compounds on carbon-doped titanium dioxide, as studied by photocurrent measurements, J. Phys. Chem. C 111 (2007) 8603–8610.
[11] Y. Huang, W.K. Ho, S.C. Lee, L.Z. Zhang, G.S. Li, J.C. Yu, Effect of carbon doping on the mesoporous structure of nanocrystalline titanium dioxide and its solar-light-driven photocatalytic degradation of NOx, Langmuir 24 (2008) 3510–3516.
[12] D.E. Gu, Y. Lu, B.C. Yang, Y.D. Hu, Facile preparation of micro-mesoporous carbon-doped $TiO_2$ photocatalysts with anatase crystalline walls under template-free condition, Chem. Commun. 21 (2008) 2453–2455.
[13] F. Dong, H.Q. Wang, Z.B. Wu, One step "green" synthetic approach for mesoporous C-doped $TiO_2$ with efficient visible light photocatalytic activity, J. Phys. Chem. C 113 (2009) 16717–16723.
[14] F. Dong, W.R. Zhao, Z.B. Wu, Characterization and photocatalytic activities of C, N and S co-doped $TiO_2$ with 1D nanostructure prepared by nano-confinement effect, Nanotechnology 19 (2008) 365607.
[15] Z.B. Wu, F. Dong, W.R. Zhao, H.Q. Wang, Y. Liu, B.H. Guan, Fabrication and characterization of novel carbon-doped $TiO_2$ nanotubes, nanowires and nanorods with high visible light photocatalytic activity, Nanotechnology 20 (2009) 235701.
[16] J.H. Park, S. Kim, A.J. Bard, Novel Carbon-doped $TiO_2$ nanotube arrays with high aspect ratios for efficient solar water splitting, Nano Lett. 6 (2006) 24–28.
[17] Z.B. Wu, F. Dong, W.R. Zhao, S. Guo, Visible light induced electron transfer process over nitrogen doped $TiO_2$ nanocrystals prepared by oxidation of titanium nitride, J. Hazard. Mater. 157 (2008) 57–63.
[18] Q. Li, R.C. Xie, Y.W. Li, E.A. Mintz, J.K. Shang, Enhanced visible-light-induced photocatalytic disinfection of E. coli by carbon-sensitized nitrogen-doped titanium oxide, Environ. Sci. Technol. 41 (2007) 5050–5056.
[19] Y.P. Peng, S.L. Lo, H.H. Ou, S.W. Lai, Microwave-assisted hydrothermal synthesis of N-doped titanate nanotubes for visible-light-responsive photocatalysis, J. Hazard. Mater. 183 (2010) 754–758.
[20] D. Mitoraj, H. Kisch, The nature of nitrogen-modified titanium dioxide photocatalysts active in visible light, Angew. Chem., Int. Ed. 47 (2008) 9975–9978.
[21] X.F. Qiu, Y.X. Zhao, C. Burda, Chemically synthesized nitrogen-doped metal oxide nanoparticles, Adv. Mater. 19 (2007) 3995–3999.
[22] F. Dong, W.R. Zhao, Z.B. Wu, S. Guo, Band structure and visible light photocatalytic activity of multi-type nitrogen doped $TiO_2$ nanoparticles prepared by thermal decomposition, J. Hazard. Mater. 162 (2008), pp. 763–760.
[23] Q. Li, J.K. Shang, Heavily nitrogen-doped dual-phase titanium oxide thin films by reactive sputtering and rapid thermal annealing, J. Am. Ceram. Soc. 91 (2008) 3167–3172.
[24] Y.X. Li, Y. Jiang, S.Q. Peng, F.Y. Jiang, Nitrogen-doped $TiO_2$ modified with $NH_4F$ for efficient photocatalytic degradation of formaldehyde under blue light-emitting diodes, J. Hazard. Mater. (2010) 90–96.
[25] J. Wang, D.N. Tafen, J.P. Lewis, Z.L. Hong, A. Manivannan, M.J. Zhi, M. Li, N.Q. Wu, Origin of photocatalytic activity of nitrogen-doped $TiO_2$ nanobelts, J. Am. Chem. Soc. 131 (2009) 12290–12297.
[26] Q. Li, Y.W. Li, P.G. Wu, R.C. Xie, J.K. Shang, Palladium oxide nanoparticles on nitrogen-doped titanium oxide: accelerated photocatalytic disinfection and post-illumination catalytic memory, Adv. Mater. 20 (2008) 3717–3723.

[27] Z.B. Wu, F. Dong, Y. Liu, H.Q. Wang, Enhancement of the visible light photocatalytic performance of C-doped $TiO_2$ by loading with $V_2O_5$, Catal. Commun. 11 (2009) 82–86.
[28] Y. Cong, J.L. Zhang, F. Chen, M. Anpo, D.N. He, Preparation, photocatalytic activity, and mechanism of nano-$TiO_2$ co-doped with nitrogen and iron (III), J. Phys. Chem. C 111 (2007) 10618–10623.
[29] X.F. Chen, X.C. Wang, Y.D. Hou, J.H. Huang, L. Wu, X.Z. Fu, The effect of postnitridation annealing on the surface property and photocatalytic performance of N-doped $TiO_2$ under visible light irradiation, J. Catal. 255 (2008) 59–67.
[30] H. Ozaki, S. Iwamoto, M. Inoue, Marked promotive effect of iron on visible-light-induced photocatalytic activities of nitrogen- and silicon-codoped titania, J. Phys. Chem. C 111 (2007) 17061–17066.
[31] H. Tada, T. Mitsui, T. Kiyonaga, T. Akita, K. Tanaka, All-solid-state Z-scheme in CdS–Au–$TiO_2$ three-component nanojunction system, Nat. Mater. 5 (2006) 782–786.
[32] H. Park, W. Choi, M.R. Hoffmann, Effects of the preparation method of the ternary CdS/$TiO_2$/Pt hybrid photocatalysts on visible light-induced hydrogen production, J. Mater. Chem. 18 (2008) 2379–2385.
[33] C. Hu, Y.Q. Lan, J.H. Qu, X.X. Hu, A.M. Wang, Ag/AgBr/$TiO_2$ visible light photocatalyst for destruction of azodyes and bacteria, J. Phys. Chem. B 110 (2006) 4066–4072.
[34] L.S. Zhang, K.H. Wong, Z.G. Chen, J.C. Yu, J.C. Zhao, C. Hu, C.Y. Chan, P.K. Wong, AgBr-Ag-$Bi_2WO_6$ nanojunction system: a novel and efficient photocatalyst with double visible-light active components, Appl. Catal. A 363 (2009) 221–229.
[35] A. Janczyk, A. Wolnicka-Glubisz, K. Urbanska, G. Stochel, W.J. Macyk, Photocytotoxicity of platinum(IV)-chloride surface modified $TiO_2$ irradiated with visible light against murine macrophages, Photochem. Photobiol. B 92 (2008) 54–58.
[36] G.Q. Li, D.F. Wang, Z.G. Zou, J.H. Ye, Enhancement of visible-light photocatalytic activity of $Ag_{0.7}Na_{0.3}NbO_3$ modified by a platinum complex, J. Phys. Chem. C 112 (2008) 20329–20333.
[37] L. Zang, C. Lange, I. Abraham, S. Storck, W.F. Maier, H. Kisch, Amorphous microporous titania modified with platinum(IV) chloride – A new type of hybrid photocatalyst for visible light detoxification, J. Phys. Chem. B 102 (1998) 10765–10771.
[38] J.C. Yu, H.Y. Yip, L. Wu, P.K. Wong, S.Y. Lai, A mesoporous Pt/$TiO_2$ nanoarchitecture with catalytic and photocatalytic functions, Chem. Eur. J. 11 (2005) 2997–3004.
[39] W.Y. Teoh, L. Madler, R. Amal, Inter-relationship between Pt oxidation states on $TiO_2$ and the photocatalytic mineralisation of organic matters, J. Catal. 251 (2007) 271–280.
[40] H.W. Chen, Y. Ku, Y.L. Kuo, Effect of Pt/$TiO_2$ characteristics on temporal behavior of o-cresol decomposition by visible light-induced photocatalysis, Water Res. 41 (2007) 2069–2078.
[41] C.H. Ao, S.C. Lee, C.L. Mak, L.Y. Chan, Photodegradation of volatile organic compounds (VOCs) and NO for indoor air purification using $TiO_2$: promotion versus inhibition effect of NO, Appl. Catal. B 42 (2003) 119–129.
[42] J.H. Mo, Y.P. Zhang, Q.J. Xu, Y.F. Zhu, J.J. Lamson, R.Y. Zhao, Determination and risk assessment of by-products resulting from photocatalytic oxidation of toluene, Appl. Catal. B 89 (2009) 570–576.
[43] J.G. Yu, S.W. Liu, H.G. Yu, Microstructures and photoactivity of mesoporous anatase hollow microspheres fabricated by fluoride-mediated self-transformation, J. Catal. 249 (2007) 59–66.
[44] R.J. Cui, C. Liu, J.M. Shen, D. Gao, J.J. Zhu, H.Y. Chen, Gold nanoparticle-colloidal carbon nanosphere hybrid material – preparation, characterization, and application for an amplified electrochemical immunoassay, Adv. Funct. Mater. 18 (2008) 2197–2204.
[45] J.W. Kim, H.G. Lee, S. Kim, The electronic state of platinum phthalocyanine studied by X-ray photoelectron spectroscopy, J. Electron. Spectrosc. 85 (1997) 35–38.
[46] H.Q. Wang, Z.B. Wu, Y. Liu, Y.J. Wang, Influences of various Pt dopants over surface platinized $TiO_2$ on the photocatalytic oxidation of nitric oxide, Chemosphere 74 (2008) 773–778.
[47] C.H. Lin, J.H. Chao, C.H. Liu, J.C. Chang, F.C. Wang, Effect of calcination temperature on the structure of a Pt/$TiO_2$ (B) nanofiber and its photocatalytic activity in generating $H_2$, Langmuir 24 (2008) 9907–9915.
[48] W. Zhao, C.C. Chen, W.H. Ma, J.C. Zhao, D.X. Wang, H. Hidaka, N. Serpone, Efficient photoinduced conversion of an azo dye on hexachloroplatinate(IV)-modified $TiO_2$ surfaces under visible light irradiation, Chem. Eur. J. 9 (2003) 3292–3299.
[49] S. Kim, S.J. Hwang, W. Choi, Visible light active platinum-ion-doped $TiO_2$ photocatalyst, J. Phys. Chem. B 109 (2005) 24260–24267.
[50] X.B. Chen, C. Burda, The electronic origin of the visible-light absorption properties of C-, N- and S-doped $TiO_2$ nanomaterials, J. Am. Chem. Soc. 130 (2008) 5018–5019.
[51] X.B. Chen, P.A. Glans, X. Qiu, S. Dayal, W.D. Jennings, K.E. Smith, C. Burda, J. Guo, X-ray spectroscopic study of the electronic structure of visible-light responsive N-, C- and S-doped $TiO_2$, J. Electron. Spectrosc. 162 (2008) 75–81.
[52] J.G. Yu, G.H. Wang, B. Cheng, M.H. Zhou, Effects of hydrothermal temperature and time on the photocatalytic activity and microstructures of bimodal mesoporous $TiO_2$ powders, Appl. Catal. B 69 (2007) 171–180.
[53] Y. Ishibai, J. Sato, S. Akita, T. Nishikawa, S. Miyagishi, Photocatalytic oxidation of $NO_x$ by Pt-modified $TiO_2$ under visible light irradiation, J. Photochem. Photobiol. A. 188 (2007) 106–111.
[54] J. Zhang, M.J. Li, Z.C. Feng, J. Chen, C. Li, UV Raman spectroscopic study on $TiO_2$. I. Phase transformation at the surface and in the bulk, J. Phys. Chem. B 110 (2006) 927–935.
[55] H. Wang, X. Quan, H.T. Yu, S. Chen, Fabrication of a $TiO_2$/carbon nanowall heterojunction and its photocatalytic ability, Carbon 46 (2008) 1126–1132.
[56] Y. Xie, K.L. Ding, Z.M. Liu, R.T. Tao, Z.Y. Sun, H.Y. Zhang, G.M. An, In situ controllable loading of ultrafine noble metal particles on titania, J. Am. Chem. Soc. 131 (2009) 6648–6649.
[57] D.Z. Li, Z.X. Chen, Y.L. Chen, W.J. Li, H.J. Huang, Y.H. He, X.Z. Fu, A new route for degradation of volatile organic compounds under visible light: using the bifunctional photocatalyst Pt/$TiO_{2-x}N_x$ in $H_2O_2$ atmosphere, Environ. Sci. Technol. 42 (2008) 2130–2135.
[58] S. Higashimoto, Y. Ushiroda, M. Azuma, H. Ohue, Synthesis, characterization and photocatalytic activity of N-doped $TiO_2$ modified by platinum chloride, Catal. Today 132 (2008) 165–169.
[59] W. Macyk, H. Kisch, Photosensitization of crystalline and amorphous titanium dioxide by platinum(IV) chloride surface complexes, Chem. Eur. J. 7 (2001) 1862–1867.
[60] J.G. Yu, M.H. Zhou, B. Cheng, X.J. Zhao, Preparation, characterization and photocatalytic activity of in situ N, S-codoped $TiO_2$ powders, J. Mol. Catal. A 246 (2006) 176–184.
[61] Y. Xu, M.A.A. Schoonen, The absolute energy positions of conduction and valence bands of selected semiconducting minerals, Am. Mineral. 85 (2000) 543–556.
[62] H.Q. Jiang, M. Nagai, K. Kobayashi, Enhanced photocatalytic activity for degradation of methylene blue over $V_2O_5$/$BiVO_4$ composite, J. Alloys Compd. 479 (2009) 821–827.
[63] M. Long, W.M. Cai, J. Cai, B.X. Zhou, X.Y. Chai, Y.H. Wu, Efficient photocatalytic degradation of phenol over $Co_3O_4$/$BiVO_4$ composite under visible light irradiation, J. Phys. Chem. B 110 (2006) 20211–20216.
[64] W. Macyk, G. Burgeth, H. Kisch, Photoelectrochemical properties of platinum(IV) chloride surface modified $TiO_2$, Photochem. Photobiol. Sci. 2 (2003) 322–328.